

Lab 6: Double Einstein Ring System SDSSJ0946+1006

Pierre Christian*

December 7th 2010

Abstract

In this lab we analyzed datasets of the double Einstein ring system SDSSJ0946+1006 from the Hubble Space Telescope archive. We found the angular separation from the lensing galaxy to the inner ring to be 1.275 ± 0.129 arcseconds and to the outer ring to be 2.464 ± 0.129 arcseconds. Using general relativity, and the previously measured redshifts and F606W magnitudes of the system, we were able to solve for the mass of the lensing galaxy using the angular radius of the inner ring. In terms of solar luminosity, the mass of the lensing galaxy was found to be $3.0217 \times 10^{11} \pm 6.11 \times 10^{10} L_{\odot}$. We were then able to solve for an upper limit of the mass to light ratio, 6.98 ± 1.41 . The high value of this upper limit convinces us of the existence of dark matter in the lensing galaxy of SDSSJ0946+1006.

1 Introduction

SDSSJ0946+1006 is a double Einstein ring system resulting from a lucky alignment of three light sources and Earth. For such an Einstein ring system, it is possible to use general relativity to relate the angular radius of the ring with the mass of the lensing galaxy. Furthermore, knowing the redshifts of

*University of California, Berkeley

the lensing galaxy and the annulus would allow us to solve said relation for the mass of the lensing galaxy completely in terms of the angular radius of the ring. This method of mass determination, coupled with photometry of the lensing galaxy, would allow us to calculate the mass to light ratio of said galaxy, thereby helping us understand the dark matter distributions of the galaxy.

For this lab, we would require Hubble Space Telescope images of SDSSJ0946+1006 taken free from atmospheric disruption, thereby possessing high enough resolution for us to resolve the lensing galaxy of the system along with its two Einstein rings. We would then analyze the image to find the angular radius of the first Einstein ring in order to measure the mass content of the lensing galaxy.

2 Theoretical Considerations

2.1 Gravitational Lensing

When light travels close to a massive object, general relativity dictates that light bends inwards towards the mass following the curvature in spacetime introduced by said mass. If an observer is to be located behind the mass (which is located behind the light source), and is positioned exactly at the straight line intersecting both the mass and the light source, the observer would see an annulus around the mass due to this bending of light. This phenomenon created what is known as an Einstein ring system. In such Einstein ring systems, the angular separation between the lensing mass and the annulus, denoted as θ , can be calculated by the equation¹:

$$\theta = \sqrt{\alpha_0 \frac{R_0}{d_L}} \quad (1)$$

Where α_0 is the angular bending of the light path as it crosses the gravitating mass, R_0 is the radius of the gravitating object (assumed to be circular), and d_L is the distance between the observer and the massive object. In such systems, however, we can solve for α_0 , resulting in θ as a function of the mass of the massive object (called the lensing object) and the three

¹Einstein, 1936: Lens-Like Action of a Star by the Deviation of Light in the Gravitational Field (Science Vol. 84, No. 2188, pg 506-507)

distances between the lensing object, the observer, and the annulus by the equation²:

$$\theta_{E1} = \sqrt{\frac{4GM(d_{S1} - d_L)}{c^2(d_{S1}d_L)}} \quad (2)$$

Where now d_{S1} is the distance between the observer and the resulting annulus, d_L is the distance between the observer and the lensing object, and M is the mass of the lensing object. In the last equation, the angular distance between the lensing mass and the Einstein ring is denoted as θ_{E1} where the subscript is used as an index shall we have multiple Einstein rings in the system. It is notable, however, that due to the small value of the gravitational constant, G , in the numerator, and the large value of the speed of light, c , in the denominator, we need a lensing object of immense mass to achieve an annulus located at a distance appreciable enough from the lensing mass that it is detectable at all using our equipments. A further complication in observing this phenomenon is the scarcity of a light source and a lensing mass that is perfectly aligned with our observers on Earth.

Miraculously, our dataset depicts a double Einstein ring system achieved using a galaxy as its final lensing object. The light from the first light source was bended by the second object, which also produced light which is bended by the final lensing galaxy. In addition, the bended light of the first light source is further bended by the final lensing galaxy. As these three objects are perfectly aligned with Earth, we can see the bending of the lights as two luminous rings encircling the final lensing galaxy, with the light from the closer lensed source forming the inner ring and light from the first light source as the outer ring.

2.2 Mass Determination of Lensing Objects

If an Einstein ring system is bright enough, spectroscopy can be used to find the cosmological redshift, z , of the annulus and the lensing object. For low redshifts ($z < 2$), the conversion between cosmological redshift and distance to Earth, d , for known Hubble constant at the current epoch, H_0 , is given by³:

²Kalas, 2010: Lab 6 - Gravitational Lensing, pg 12

³Kalas, 2010: Lab 6 - Gravitational Lensing, pg 12

$$d \sim \left(\frac{c}{H_0} \right) \left(\frac{(z+1)^2 - 1}{(z+1)^2 + 1} \right) \quad (3)$$

As such, for bright Einstein ring systems, both the distances between the observer and the lensing object, and between the observer and the annulus, can be measured. If additionally the angular separation between the lensing object and the annulus is measured, we can use the two distances and Equation (2) to solve for the mass of the lensing galaxy.

3 Equipment and Observation

3.1 Hubble Space Telescope

The Hubble Space Telescope (HST) utilizes a 2.4 meter primary mirror orbiting at 559 km from the ground to take images free from atmospheric distortion. Our dataset made use of the now retired Wide Field and Planetary Camera 2 (WFPC2), consisting of three Wide Field Cameras (WF1, WF2, and WF3) and one higher resolution, but correspondingly smaller field of view Planetary Camera (PC). All four cameras contained an 800x800 pixels CCD detector. The three Wide Field Cameras possess a plate scale of 0.1 arcsec/pixel, while the Planetary Camera possess a finer plate scale of 0.046 arcsec/pixel.

3.2 Observation

Our dataset were obtained from the online Hubble archive⁴. We selected four datasets of SDSSJ0946+1006 taken using HST's WFPC2 camera utilizing the F606W filter. These datasets have HST proposal ID 11202 and PI Leon Koopmans of the Kapteyn Astronomical Institute. For all datasets, we chosed to download the pipeline calibrated version, meaning that our images were already corrected for flat fields, geometric distortions (such as vigneting), dark counts, and bias.

Our field consisted of observations from four cameras of the WFPC2. The three Wide Field Cameras are arranged to have an 'L' shaped field of view, measuring 160 arcseconds across its two long edges. Nestled at the

⁴at <http://archive.stsci.edu/hst/>

top right corner of this field is the smaller field of view of the Planetary Camera, a box measuring 36.8 arcseconds across. Our target, the Einstein Ring System SDSSJ0946+1006, was captured within the field of WF3 located at the bottom left corner of the entire WFPC2 field of view.

The observation, conducted on December 17 2007 at 21:06:17 UT, utilizes the F606W filter which spans 1502 angstroms about 5997 angstroms. The integration time used was 1100 seconds.

3.3 Cosmic Rays and Sky Background

In order to reject cosmic rays, we coadded our four images together by taking the median of each pixels of the four images. Since it is improbable for cosmic rays to hit the same pixels on more than one of our images, by taking the median we could effectively remove them. In practice, before we coadd them in this manner, we have to first align the four images. This is because HST's revolution around the Earth caused an apparent movement of the Einstein ring system between each exposures. Despite HST's automatic tracking system, the pixel location of our target differs considerably between the images.

In order to align the images, we first determine the centroid pixel positions of the lensing galaxy of all four images using the IRAF command `imcntr`. The values are presented in Table 1. Also presented in the table are the differences between the galaxy's centroid of a particular image and the galaxy's centroid in the first image. Shifting the second, third, and fourth images by these differences would effectively align them with the first image. In practice, these alignments are done using IRAF's `imshift` command.

Image Number	x Pos (Pix)	y Pos (Pix)	x-difference (Pix)	y-difference (Pix)
1	366.475	376.860	0	0
2	371.486	379.296	-5.01	-2.43
3	374.011	384.322	-7.54	-7.46
4	369.008	381.885	-2.53	-5.03

Table 1: Pixel centroid position of the lensing galaxy in the four images. The x-difference and y-difference columns corresponds to the differences of the centroid positions between the image and the first image.

The median coaddition of the first image and the shifted second, third, and fourth images was then done using IRAF's imcombine utilizing the comb=median keyword. The mean, median, mode, and standard deviation of a small empty region (at [125:174, 135:184] can be obtained for our images using IRAF's imstat package (utilizing the field keyword). The statistics for four of our original images, along with their average value, are listed in Table 2. The same statistics, this time calculated for the combined image, are listed in Table 3. Note that the standard deviation of the combined image is lower by a factor of ~ 9.5 from the average of the four single images. This corresponds to the coaddition reducing the sky background noise.

Image Number	Mean (ADU)	Median (ADU)	Mode (ADU)	Stddev (ADU)
1	0.02035	0.01934	0.0193	0.0122 mmmm
2	0.02216	0.02178	0.02169	0.0040
3	0.01962	0.01927	0.01949	0.0040
4	0.02273	0.02176	0.02164	0.0072
Average	0.02122	0.02054	0.02053	0.00685

Table 2: Image statistics for the four exposures, taken at a small, empty region at position [125:174, 135:184].

Image	Mean (ADU)	Median (ADU)	Mode (ADU)	Stddev (ADU)
Combined	0.0206	0.02053	0.02027	7.2×10^{-4}

Table 3: Image statistics of the median coadded image, taken at a small, empty region at position [125:174, 135:184]. Note that the standard deviation drops by ~ 9.5 from the average of the single images.

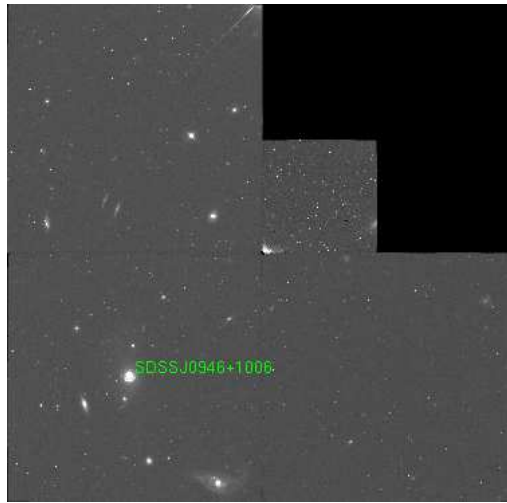
Also notable from Table 3 is that although the HST is located above the atmosphere, therefore exempt to sky background due to light reflecting off the atmosphere, the median of the empty region is not zero. This means that our HST data is still polluted by some sky background. Some cause of this light pollution is the reflection of sunlight by dust in the zodiacal cloud: a thin, flat, dust cloud located within the solar system. Nevertheless, we would

need to remove this sky background by subtracting our coadded image by the median data number of an empty patch of sky. This was achieved by using IRAF's imarith to subtract the median listed in Table 3 from our coadded image. The resulting image is shown in Figure 1 (a). Shown in Figure 1 (b) is the magnified field of view of WF3.

4 Resulting Image

In Figure 1 (b), E denotes a bright star that we used to get our experimental point spread function. The FWHM of the star, measured using IRAF's radprof package, denotes the angular resolution of the image in the bandpass. The pixel FWHM obtained for this star is 2.64 pixels. Converting this into arcseconds using the plate scale (0.1 arcseconds per pixel), we get the angular resolution of the image to be 0.264 arcseconds. The theoretical best angular resolution for a telescope is given by $\sim \frac{\lambda}{D}$ where λ denotes the wavelength observed and D denotes the diameter of the telescope. Plugging in the center wavelength of our bandpass, 599.7 nm, and the diameter of the HST, 2.4 m, we get a theoretical best angular resolution of 0.0515 arcseconds. Therefore, our achieved angular resolution is 5.122 times larger than the theoretical best. This meant that although the HST is free from atmospheric disturbances, it still fail to attain the best possible angular resolution. This can be due to the diffraction of its apperture which worsen its angular resolution by a geometric factor, or imperfections in the mirror itself.

Besides the Einstein ring system, the field of Figure 1 (b) is also littered with various other interesting objects. A, B, C, and D, for example, are other galaxies. If spectras are taken for each of those galaxies, we would be able to measure their cosmological redshifts. By equation (2), we would then be able to find their distances from Earth. With this information, it is possible to figure out if all five galaxies are located close to each other in 3-D space, or if only their 2-D projections are near each other (since our image only showed their 2-D projection). We can then discern how many of those galaxies are gravitationally affecting each other. If we can measure their velocity vectors, we would then be able to discern if any of them form gravitationally bound systems. Another interesting note is that galaxy A possess extended features that looks disturbed. This hints that galactic interactions (such as galactic collisions) happened to galaxy A in the past. It would be interesting to observe galaxy A through a different bandpass. If it is the subject of a



(a)



(b)

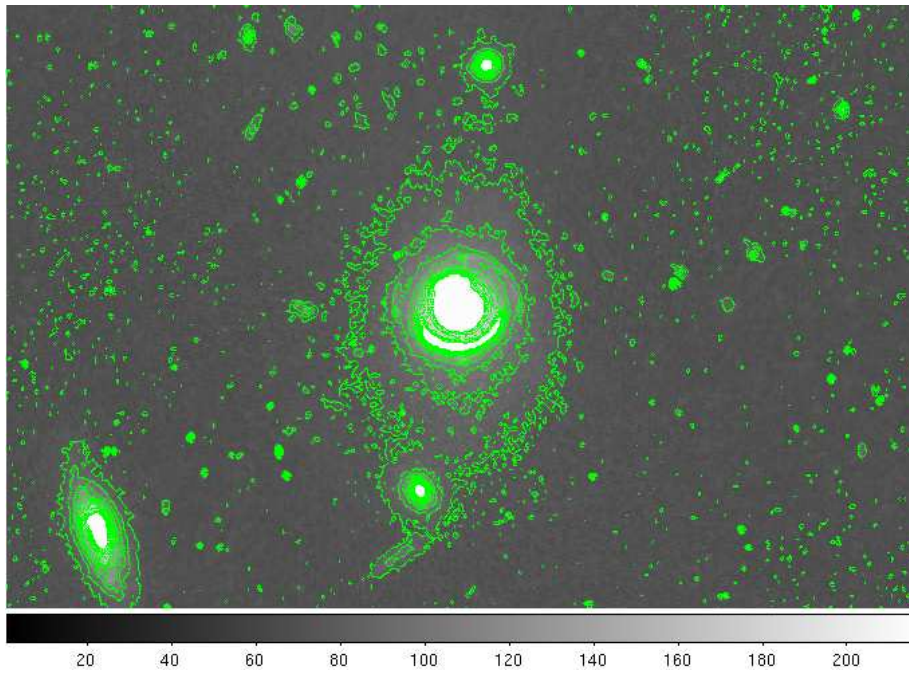
Figure 1: (a) Shows the entire field of our WFPC2 SDSSJ0946+1006 dataset after cosmic ray and sky background rejection. The three large boxes arranged like an 'L' are the Three WFC camera field of views. Each of the box measure 80 arcseconds across. The smaller box at top right corner is the PC field of view measuring 36.8 arcseconds across. (b) Shows the magnified field of view of WF3, where our target Einstein ring system resides. The letter labels A-E denotes other interesting objects in the field.

galactic collision, for example, perhaps we can see a trail of hot gaseous matters which leads to the direction the other galaxy went after the collision if we look at the field through a different wavelength range. Due to the rarity of lensing events, it would be improbable to find another Einstein ring system in the field. Looking through the other objects closely confirmed this. None of the other objects displayed any morphology that bends or curves the way an Einstein annulus does. In the most cases, objects in the field possessed morphology that are circular or elliptical. Some of the smaller dots are actually cosmic rays that survived our cosmic ray rejection method. This was ascertained by blinking through the four single images in ds9. Many of the smaller dot features appear in two consecutive images but not in the rest, a tell tale sign of cosmic rays.

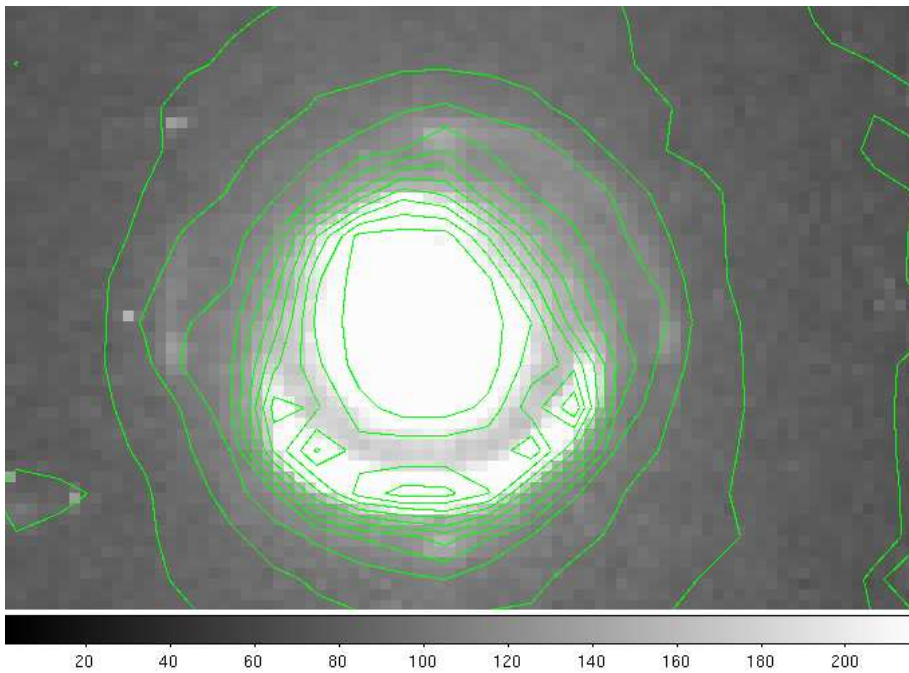
The contour plot of the field surrounding our target Einstein ring system is shown in Figure 2 (a). The same plot zoomed into our target Einstein ring system is shown in Figure 2 (b). Notice the large elliptical structure in Figure 2 (a). This structure, which is not apparent without the contour lines, are the galaxy isophotes of the fainter, extended region of the galaxy. In Figure 2 (b), an interesting note is that the isophote of the central portions of the lensing galaxy rotates as the radius increases. Therefore, it is as if the lensing galaxy is made of two parts, a central, smaller but brighter part, and an extended, large but faint part. Using IRAF's `imcntr`, we calculated the centroid position of the lensing galaxy to be $[366.475, 376.860]$. Furthermore, using the IRAF package `radprof`, we were able to calculate the FWHM of the galactic center to be of 4.98 pixels, or 0.498 arcseconds. Using the same method, the semimajor axis of the extended part of the galaxy is measured to be 52.5 pixels, while the semiminor axis is 36 pixels. Multiplying by the plate scale, these numbers corresponds to 5.25 and 3.6 arcseconds respectively.

5 Galaxy Subtraction

For the purpose of emphasizing the lenses' structures, we can remove the lensing galaxy from our coadded image. This removal can be done by first modelling the galaxy and then subtracting this model galaxy from our coadded image.



(a)



(b)

Figure 2: (a) Shows the contour plot of the field surrounding SDSSJ0946+1006 after cosmic ray and sky background rejection. Note the large elliptical structure that extends further from the directly apparent region of the galaxy. This fainter portion of the galaxy is due to the galaxy's extended regions. (b) Shows the same contour plot as (a) magnified to emphasize the central parts of SDSSJ0946+1006. Note the isophote's twisting (rotating) as it increases radius.

5.1 de Vaucouleurs' Model Galaxy

A simple elliptical galaxy model that we used in modelling the lensing galaxy was the de Vaucouleurs' model. The de Vaucouleur profile describes the surface brightness, I , of an elliptical galaxy as a function of the galactic radius, R , as⁵:

$$\ln I(R) = \ln I_0 - kR^{1/4} \quad (4)$$

Where I_0 is the surface brightness at the center of the galaxy and k is a proportionality constant. Defining R_e as the radius where half the luminosity of the galaxy is contained, we can eliminate the proportionality constant k to write the de Vaucouleur profile as:

$$\ln I(R) = \ln I_e + 7.67 \left(1 - \left(\frac{R}{R_e} \right)^{\frac{1}{4}} \right) \quad (5)$$

As such, a de Vaucouleur elliptical galaxy can be completely specified by its magnitude, semimajor axis, and axial ratio (semimajor divided by semiminor axis), as well as its position coordinates and position angle describing the galaxy's location and rotation placement in the field.

5.2 Galaxy Modelling and Subtraction Method

Our de Vaucouleur galaxy can be modelled using IRAF's mkobject package. This package allowed the creation of images based on various theoretical models. In this case, we used mkobject to construct a de Vaucouleur galaxy by feeding it a text file containing the centroid position, the magnitude, the name of the galaxy model, the semimajor axis, the axial ratio, and the position angle of the model galaxy. To model our galaxy, due to the profile of the galaxy isophotes described in section 4, we have to superimpose two de Vaucouleur galaxies. The first component would be a brighter galaxy that would model the central parts of our lensing galaxy. The second component would be a fainter galaxy to model the extended portions of our lensing galaxy. The parameters which goes into building these two galaxies are given in Table 4. The centroid positions of both galaxy components are the centroid position of our lensing galaxy [366.475, 376.860].

Magnitude	Semimajor Axis (Pix)	Axial Ratio	Position Angle (degrees)
2	20	0.95	5
5	20.2	0.9	80

Table 4: Parameters of the two de Vaucouleur galaxies used to model our lensing galaxy. The first entry described a brighter galaxy that models the central portions of our lensing galaxy while the second entry described a fainter one that models the extended features of our lensing galaxy.

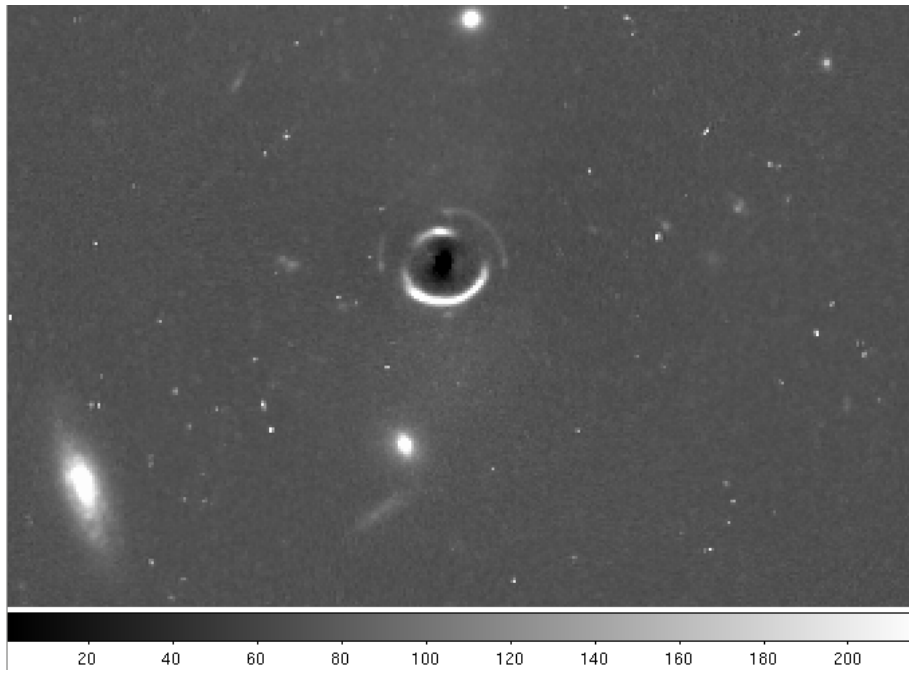
Our model galaxy can then be subtracted from the coadded image using IRAF’s imarith’s image subtraction. The resulting image of our target Einstein ring system, is shown in Figure 3 (a) while the contour plot is shown in Figure 3 (b). Note that in Figure 3 (b), the large elliptical contours of the galaxy’s extended portion is absent. Thus, this model works very well in the extended part of our lensing galaxy. The black patch at the central regions of the galaxy, however, indicates that our model had oversubtract on some center parts of the lensing galaxy. This is because the central portions of the lensing galaxy was not completely elliptical, while our model for the center of the galaxy is a perfectly elliptical object. As the ellipse of our model galaxy thus covers more than the entire galactic center, some parts of the galaxy center was oversubtracted by our model galaxy. Also note that in contrast with Figure 2 (b), the upper portion of the inner Einstein ring is very apparent.

6 High Pass Filtering

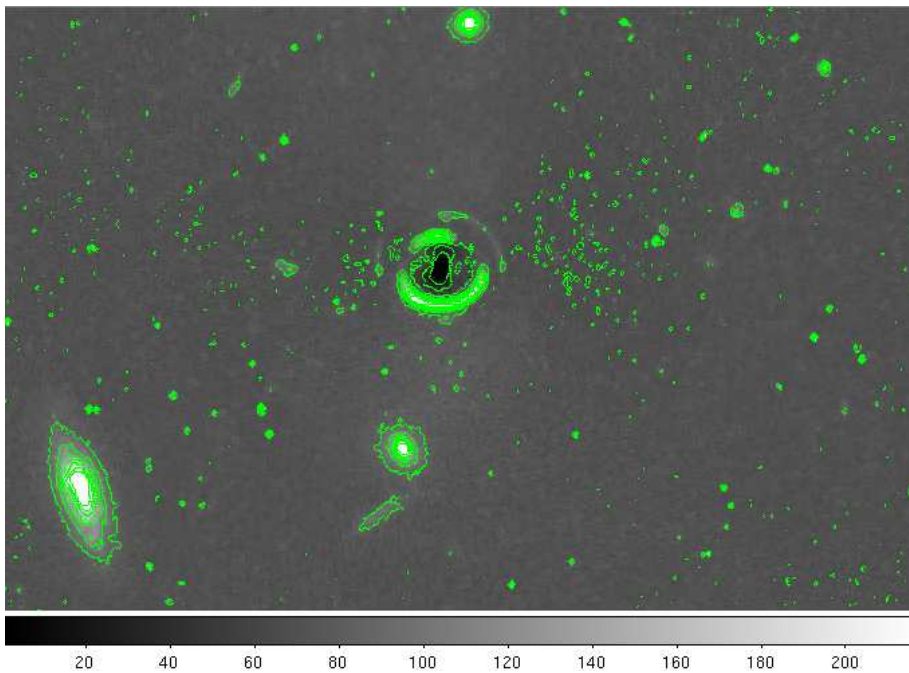
Putting an image through a high pass filter would remove low resolution structures. In effect, broad objects such as the extended morphology of the lensing galaxy would be deemphasized while smaller details such as stars or the core of a galaxy would be accentuated. By passing our image through a high pass filter, we therefore can increase the apparent sharpness of the image without actually obtaining new data.

In this lab, the high pass filter was made by convolving our coadded image with a gaussian function using the IRAF package gauss. This convolution results in a copy of our image that is deliberately blurred, where the extend

⁵Caroll & Ostlie, 1996: Modern Astrophysics, pg. 928



(a)



(b)

Figure 3: (a) Shows SDSSJ0946+1006 after we subtracted our model galaxy. Note that the center galaxy is over-subtracted. This is due to the center of the galaxy not being a perfect ellipse, while our model for the center of the galaxy is a perfectly elliptical object. (b) Shows the contour plot of the galaxy. Note that in contrast to the contour plot before the model galaxy subtraction, the large elliptical isophotes due to the extended portions of the galaxy is missing. This shows that our model is a good fit for the extended regions of the galaxy.

of the blurring depends on the standard deviation of the gaussian (increasing the standard deviation of the gaussian would blur the image more). We then used IRAF's imarith to subtract our coadded image with its convolved copy. As the convolved image is essentially a low pass filter, the subtraction would cancel the low resolution structures (which are practically unaffected by the convolution) almost completely while leaving the high detailed structures intact. The choice of gaussian σ reflects how sharp the resulting high pass filtered image would be. A larger σ would increase the frequency threshold that would not pass the filter. As such, choosing a higher σ would amount to increasing the apparent sharpness of the resulting high pass image. We chose $\sigma = 5$ as a compensation between sharpening the image enough to remove the extended morphology of the galaxy, while still passing as much information as possible (since at very high frequency filters, even the rings would be filtered, changing their shapes significantly). Our target Einstein ring system after applying high pass filtering of gaussian $\sigma = 5$ is depicted in Figure 4. As seen, the extended structures of the galaxy are removed and the smaller details (such as the lensing galaxy center and the rings) are emphasized. In contrast with Figure 2 (b), for example, the upper portion of the inner Einstein ring is clearly visible.

7 Astrometry

The radial angular separation between the lens galaxy and the rings were done by plotting a cut of the image using IRAF's graph package. A vertical radial cut was made across the Einstein ring system at pixel 368 horizontally and between pixel 343 to 405 in the vertical direction of the high pass filtered image (the dotted line in Figure 4).

The resulting radial cut, plotting pixel in the vertical direction versus the data number is shown in Figure 5. In the figure, the large peak with centroid at pixel 35.2 ± 1.29 corresponds to the center of the lensing galaxy, where the uncertainty due to the centroid method is obtained by taking 200 centroid calculations with different starting position (determined in IDL using the cursor function) and taking the standard deviation of the results. The two smaller dips with centroid positions at 21 pixel and at 46.5 corresponds to the light emissions of the inner ring, while the even less pronounced dip at pixel 58.5 is due to the outer ring. Since they were all calculated with the same centroid function, they all carry the same uncertainty of ± 1.29

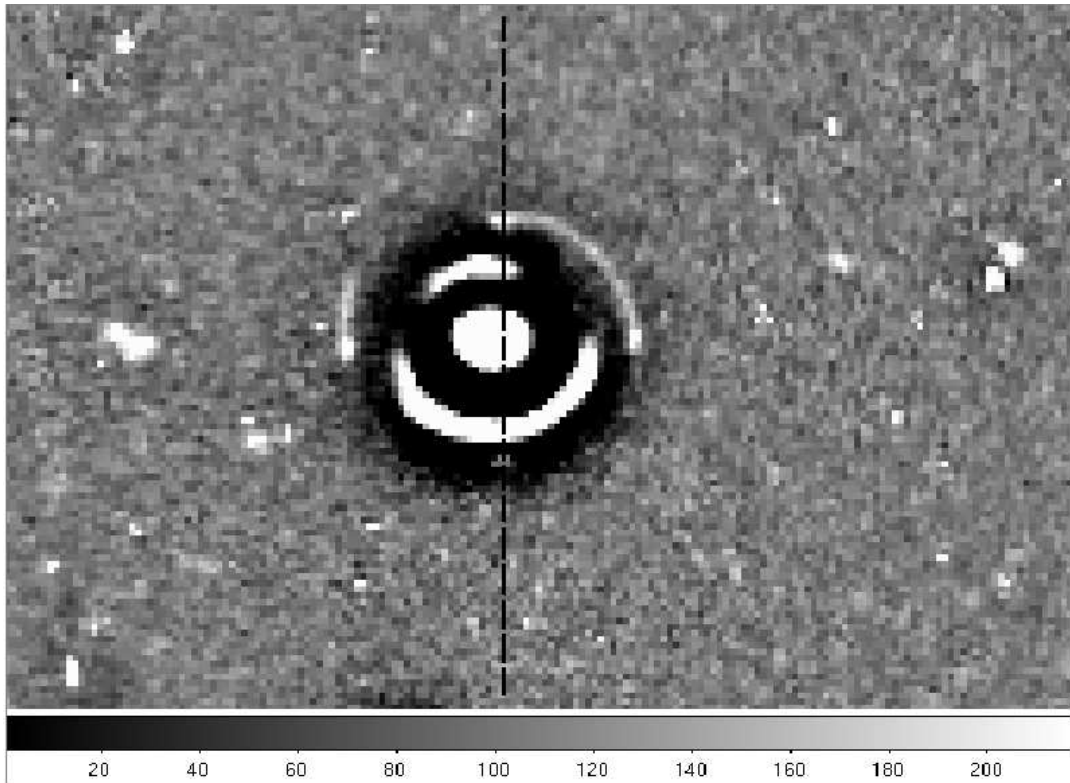


Figure 4: SDSSJ0946+1006 after high pass filtering. We convolved our coadded image with a gaussian of $\sigma=5$ and subtract this convolution from the original image, creating a high-passed image. Note that the central portion of the galaxy and the rings are accentuated. The dotted lines corresponds to the cut done to produce a pixel vs. data number plot in the Astrometry section.

pixels. The absolute pixel differences between the centroids of the inner ring emissions and the central galaxy emission are therefore 14.2 ± 1.29 pixels (to the upper ring) and 11.3 ± 1.29 pixels (to the lower ring). Averaging these two pixel regress gives the mean pixel annulus of the inner ring to be 12.75 ± 1.29 pixels. Multiplying this number by the plate scale of WF3, 0.1 arcsec/pixel, we get the angular separation of the inner annulus to be 1.275 ± 0.129 arcseconds. We can confidently detect only one side of the outer ring emission, due to it being fainter. The pixel difference between the centroid of the central galaxy and the centroid of the outer ring emission is 23.3 ± 1.29 pixels. Again, multiplying this number by the plate scale of WF3 gives us the angular separation of the outer annulus to be 2.33 ± 0.129 arcseconds.

If we are to use, instead of the high pass filter, the model galaxy subtracted image from the previous section, we would gain another method by which we can calculate the rings' radial angular separation. Taking a radial cut of the image at the same location, we would obtain the same centroid positions for the rings' emissions. However, we would need a new method to find the center of our lensing galaxy. Since our model galaxy succeeded in canceling out the actual galaxy, then the location of the galaxy's center should be located at the position we placed the center of the model galaxy [366.475, 376.860]. The vertical position of our galaxy is therefore 376.860. This corresponds to pixel number 33.86 in Figure 5 (the image in Figure 5 starts at pixel 343, therefore, the pixel position of the model galaxy in Figure 5 is pixel number $376.860 - 343 = 33.86$). The absolute pixel differences between this new centroid and the two inner ring emission lines visible in Figure 5 are 12.86 (for the distance to the upper ring) and 12.64 (for the distance to the lower ring). Since the rings' emission centroids still carry the centroid uncertainty, these values have uncertainty of ± 1.29 pixels. The average of these values again give us the average pixel angular separation of the inner annulus to be 12.75 ± 1.29 pixels, or multiplying by the plate scale, 1.275 ± 0.129 arcseconds. Doing the same procedure with the single outer ring centroid give the angular separation of the outer ring to be 24.64 ± 1.29 pixels, or multiplying by the plate scale, 2.464 ± 0.129 arcseconds. The fact that we get similar answers using both methods means that for the purposes of this lab, it does not really matter which method were used in subtracting the lensing galaxy.

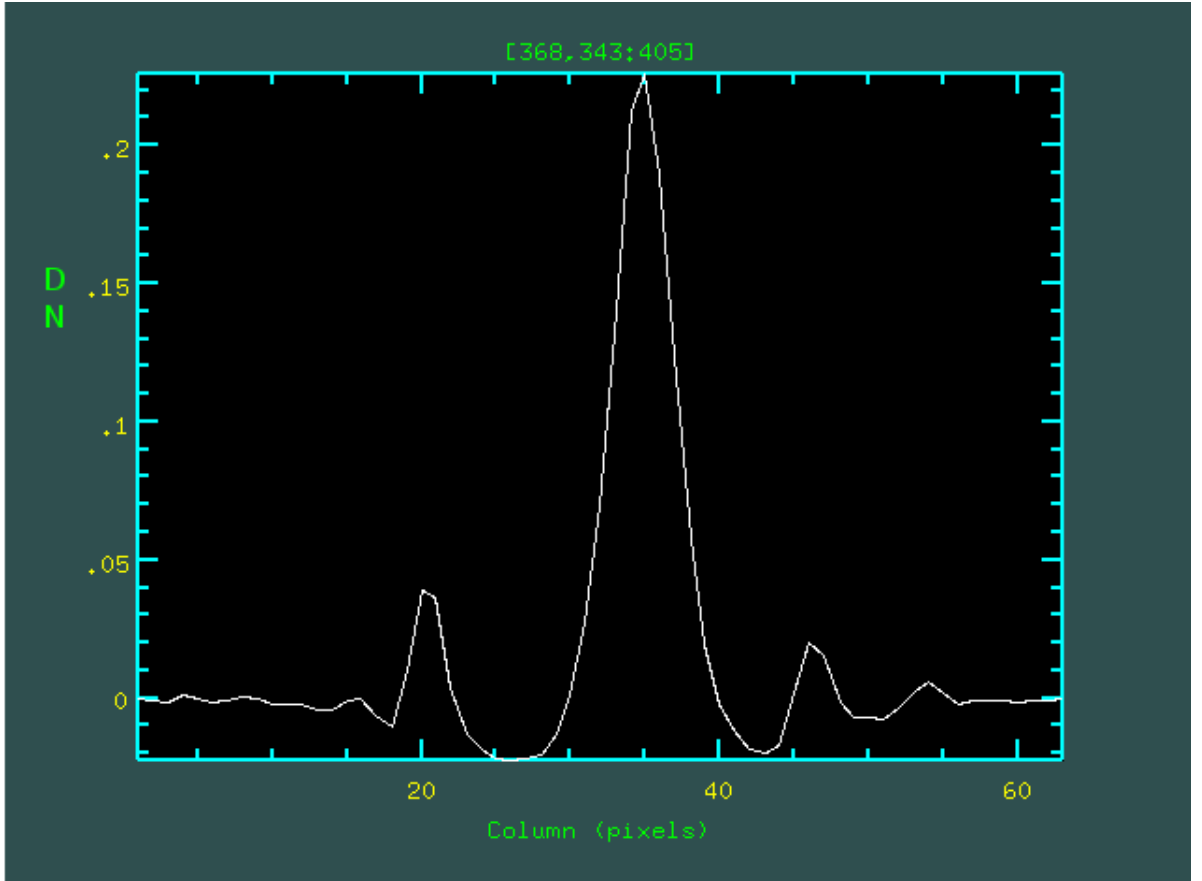


Figure 5: Plot of pixel in the vertical direction versus data number of SDSSJ0946+1006. This image was made by making a vertical cut across the Einstein ring system at [368, 343:405] (depicted as the dotted line across Figure 4) of the high pass filtered image. Note the large peak at 35.2 pixel due to the center of the lens galaxy, the two smaller peaks at 21 and 46.5 due to the inner ring, and the even smaller peak at 58.5 due to the outer ring.

8 Dark Matter Analysis

The redshifts to the lensing galaxy and the inner ring are known to be 0.222 and 0.609 respectively (the outer ring is too faint for redshift measurements). By the methods of section 2.2, we could use this information, along with the angular separation of the first ring obtained in the previous section, to solve for the mass of the lensing galaxy. Using equation (3), and the WMAP value of H_0 (71 (km/sec)/Mpc), we calculated the distance between Earth and the lensing galaxy to be 835.97 Mpc and the distance between Earth and the inner ring to be 1870.66 Mpc.

The mass of the galaxy can be solved from equation (2) to be:

$$M = \frac{\theta_{E1}^2 c^2 (d_{S1} d_L)}{4G(d_{S1} - d_L)} \quad (6)$$

The uncertainty of the measurement can be found using the error propagation equation⁶: for an observable $I(F_1, F_2, \dots, F_N)$, the error, δI is given by:

$$\delta I = \sqrt{\left(\frac{\partial I}{\partial F_1} \delta F_1\right)^2 + \dots + \left(\frac{\partial I}{\partial F_N} \delta F_N\right)^2} \quad (7)$$

Where in this case the equation reduces to:

$$\delta M = \sqrt{\left(\frac{\partial M}{\partial \theta_{E1}} \delta \theta_{E1}\right)^2} \quad (8)$$

Where $\delta \theta_{E1}$ is the uncertainty in the angular separation between the first ring and the center of the lensing galaxy. From equation (6):

$$\frac{\partial M}{\partial \theta_{E1}} = \frac{2\theta_{E1} c^2 (d_{S1} d_L)}{4G(d_{S1} - d_L)} \quad (9)$$

And therefore the error propagation equation reads:

⁶Taylor: An Introduction to Error Analysis

$$\delta M = \left| \frac{2\theta_{E1}c^2(d_{S1}d_L)}{4G(d_{S1} - d_L)} \right| \delta\theta_{E1} \quad (10)$$

Equation (6) and (10) gives the mass of the lensing galaxy to be $3.0217 \times 10^{11} \pm 6.11 \times 10^{10} M_{\odot}$.

There are two ways to measure the luminosity of the lensing galaxy. The first is to assume that the entirety of our galactic mass is in the form of Sun-like stars. As such, the total luminosity of the galaxy, L_g would be given by:

$$L_g = \frac{M_g}{M_{\odot}} \times L_{\odot} \quad (11)$$

Where M_{\odot} and L_{\odot} are the mass and luminosity of the sun, respectively, and M_g is the mass of the galaxy. In this case the error propagation equation (7) reduces to:

$$\delta L_g = \frac{L_{\odot}}{M_{\odot}} \times \delta M_g \quad (12)$$

Equation (11), used along with the error propagation equation (7), gives the luminosity of the galaxy if the entirety of its mass is in the form of Sun-like stars to be $3.0217 \times 10^{11} \pm 6.11 \times 10^{10} L_{\odot}$.

This assumption is innacurate because the lensing galaxy is an elliptical galaxy, which typically consists of mostly old red stars, while the star is of a relatively younger yellow G-dwarf star population. Furthermore, this assumption neglects the fact that the galaxy's luminosity in this bandpass can also come in the form of non-stellar masses, such as hot interstellar gases. The most interesting error of this calculation, however, is that it does not take into account dark matter, which contributes to the mass but not to the luminosity of the galaxy.

The second way to measure the luminosity of the lensing galaxy would be to perform photometry on the lensing galaxy. Due to time constraints, we were not able to conduct the photometry ourselves. Fortunately, the apparent magnitude, m_g , of the lensing galaxy is known to be 17.78 mag in

our bandpass (F606W). Using the distance modulus, we can calculate the absolute magnitude, M_g of the galaxy by⁷:

$$M_g = m_g - 5 \log_{10} \left(\frac{d}{10 \text{pc}} \right) \quad (13)$$

Where d , the distance to the lensing galaxy, was obtained using the measured redshift to the galaxy and equation (3) to be 835.97 Mpc. This equation gives the absolute magnitude of the lensing galaxy in the F606W bandpass to be -21.830 mag. We can then calculate the luminosity of the galaxy in the bandpass, L_g , in terms of the Sun's luminosity, L_\odot , using the equation:

$$M_g = M_\odot - 2.5 \log_{10} \left(\frac{L_g}{L_\odot} \right) \quad (14)$$

Where the absolute magnitude of the sun, M_\odot , is known to be 4.76 mag. Solving for L_g in this equation gives:

$$L_g = L_\odot \times 10^{\frac{M_\odot - M_g}{2.5}} \quad (15)$$

This gives the luminosity of the lensing galaxy in the bandpass to be $4.329 \times 10^{10} L_\odot$. Note that this result is much smaller than if we assume that the mass of the galaxy consists of entirely Sun-like stars (By a factor of 6.98). This is due to two factors: the first is that our first luminosity calculations does not take into account the fact that a large portion of the galactic mass does not radiate in the same way as the sun (because some of the luminous matter might be non-stellar objects, such as hot gas, and most of the stellar objects in the elliptical galaxy would be old, red stars). The second factor is because most of the mass of the elliptical galaxy is in the form of non-luminous dark matter.

The mass to light ratio of the lensing galaxy, defined as its mass in solar mass divided by its luminosity, can be calculated using the luminosity found using the second method to be 6.98 ± 1.41 where the uncertainty follows from equation (7). The mass to light ratio gives a picture of the amount of mass that does not radiate photons (at least within the bandpass). As such, it is

⁷Caroll & Ostlie, 1996: Modern Astrophysics, pg. 68

a measure of how much dark matter is in the galaxy. Since our mass to light ratio is > 1 , we can confidently say that we detected the presence of dark matter in the lensing galaxy. However, we have assumed that all luminous objects radiates exclusively within the F606W bandpass as our luminosity is calculated using the magnitude of the lensing galaxy within the F606W bandpass only. Therefore, any objects that radiates outside the bandpass would increase our mass to light ratio despite not being dark matter. In particular, we have overcounted the amount of dark matter by adding luminous matter that radiates outside our bandpass. This means that our mass to light ratio is merely an upper limit, if there exist any material in the galaxy that radiates outside our bandpass, the mass to light ratio would lower. For example, since stars radiate in a manner very similar to blackbody radiation, it would radiate a finite amount of energy at every wavelength. Therefore, some of their luminosity must be radiated outside of the F606W bandpass.

9 Conclusion

Using the Hubble Space Telescope data achieve, we were able to obtain datasets of the double Einstein ring system SDSSJ0946+1006 and solve for the angular separation of the inner ring and the lens galaxy. By the tenets of general relativity, we were able to use this information, along with the known redshifts and magnitudes of the system to find an upper limit of the mass to light ratio, 6.98 ± 1.41 . The high value of this mass to light ratio allowed us to be confident in stating that we have found dark matter in the lensing galaxy of SDSSJ0946+1006. A concern of this lab is the large uncertainty we obtained (20% for the mass to light ratio). Most of this uncertainty comes from the uncertainty of the angular separation due to the centroid function. Therefore, in analyzing future datasets, it would be beneficial to use a better method to find the center of an emission line (such as gaussian or polynomial fitting). Nevertheless, this lab allowed us to observe firsthand the curvature of spacetime due to massive objects, as well as using this curvature to confirm the existence of the exotic dark matter.

10 Appendix: Double Einstein Ring Geometry